

# A Spectrometer to Study Elastic and Diffractive Physics at LHC

M.Arneodo, S.Maselli, C.Peroni  
INFN and University of Torino

December 2, 2024

## Abstract

The possibility to study elastic and diffractive physics in  $pp$  collisions at LHC is discussed. For this purpose we have considered detectors close to the beam in conjunction with the magnetic elements of the accelerator to provide a high precision spectrometer for very forward final state protons. The geometrical acceptance is given and the momentum resolution is calculated for different spatial resolution detectors.

## 1 Introduction

Elastic and diffractive scattering processes are generally interpreted in terms of Pomeron ( $P$ ) exchange [1]. They are characterized by a final state which contains particles emitted at very small angles with respect to the incoming beam and carry a substantial fraction of the available energy. At collider experiments these particles escape undetected down the beam pipe. The Roman pot technique [2] allows to position detectors directly in the vacuum pipe at a very small distance from the beam.

Since 1960 elastic and diffractive scattering processes have been studied in hadron-hadron interactions at CERN [3] and elsewhere. Diffractive events in deep inelastic  $ep$  scattering have been also measured at HERA [4]. Within the ZEUS experiment, the

Leading Proton Spectrometer (LPS) [5] has been built to measure the protons scattered at very small angle with respect to the incoming beam direction.

In this paper we investigate the possibility to study elastic and diffractive events in  $pp$  collisions at LHC energy ( $\sqrt{s} = 14$  TeV). In particular we study single diffractive events characterized by one of the protons emerging from the interaction isolated in rapidity and with its momentum very close to that of the beam while the other diffracts into a state of mass  $M_X$ . The Feynman graphs of the interaction are shown schematically in Fig.1. Preliminary studies on this process are presented in [6]. A full acceptance detector could be built in the last free LHC intersection region (IP4) where one could have low luminosities, of the order of  $10^{30}$  cm<sup>-2</sup> s<sup>-1</sup>. An experimental apparatus for the complete forward region has been discussed in [7], [8] and [13].

In the following we present the simulation of spectrometers in the very forward region along one of the two outgoing proton beam arms at a sufficient distance from the interaction point in order to accept final state particles produced at very small angle with respect to the incoming proton beam direction. The present paper is an extended and improved version of [9].

## 2 Simulation of elastic and diffractive $pp$ events

The process under study is the reaction  $pp \rightarrow pX$  (Fig.1) in which one of the protons remains intact and loses a small fraction of its momentum  $1 - x_L$ , with  $x_L = \frac{|p'|}{|p|}$ , where  $p$  and  $p'$  are the incoming and outgoing proton momenta, respectively. This quantity is related to the mass  $M_X$  of the hadronic system produced in the interaction by the relation:

$$\xi = 1 - x_L = \frac{M_X^2}{s},$$

where  $s$  is the square of total centre of mass energy. Elastic scattering is characterized by  $x_L = 1$  while diffractive processes dominate for  $x_L > 0.9$ . The transverse momentum  $p_T$  of the scattered proton is generally small:  $p_T \leq 1$  GeV/c.

In order to select the possible regions along the proton beam line where these processes can be studied, we need to examine in detail the properties of the proton beam and the geometrical restrictions imposed by the vacuum pipe.

Two possible ways to study the beam profile as it proceeds through the magnetic elements are summarized in the following. The first method makes use of the beta function  $\beta$  and the phase advance  $\Delta\mu$  parameters extracted directly from the LHC MAD tables [10]. The transverse distance in the bending plane of a particle from the nominal beam,  $x$ , and its angle  $\theta_x$  with respect to the nominal beam direction can be expressed as:

$$x(l) = \sqrt{\frac{\beta_x(l)}{\beta_x(0)}} \cos\Delta\mu x(0) + \sqrt{\beta_x(l)\beta_x(0)} \sin\Delta\mu \theta_x(0) + \xi D_x, \quad (1)$$

and

$$\theta_x(l) = \frac{-1}{\sqrt{\beta_x(l)\beta_x(0)}}(\sin\Delta\mu + \alpha_x(l)\cos\Delta\mu)x(0) + \sqrt{\frac{\beta_x(0)}{\beta_x(l)}}(\cos\Delta\mu - \alpha_x(l)\sin\Delta\mu)\theta_x(0) + \xi D'_x, \quad (2)$$

where

$$\alpha_x(l) = -0.5 \frac{d\beta_x}{dl} \quad (3)$$

and  $D$  is the dispersion. In the case of elastic scattering  $\xi$  is the natural beam momentum spread of  $10^{-4}$ .

The position and angle of the particle at the interaction point are indicated as  $x(0)$ ,  $\theta_x(0)$ . Here  $l$  is the coordinate along the beam path. Similar equations can be written for the  $y$  plane. Results using this method are given in [8] and [13].

The second way to look at the beam profile is to use the transport matrices of the beam line:

$$\begin{pmatrix} x(l) \\ \theta_x(l) \end{pmatrix} = \begin{pmatrix} H_{11} & H_{12} \\ H_{21} & H_{22} \end{pmatrix} \begin{pmatrix} x(0) \\ \theta_x(0) \end{pmatrix}, \quad (4)$$

where the matrix elements  $H_{ij}$  are functions of  $x_L$  only.

Fig.2 shows a possible layout for an insertion in intersection region IP4 at LHC which is consistent with the constraints imposed by the experimental magnets and RF cavities [8] and [14]. The experimental equipment for the detection of very forward scattered protons may be located in Roman pots inside the vacuum beam pipe. Tables 1,2,3 list the main features of the magnetic elements of one of the outgoing arms, from the interaction point up to 450 m.

Fig.3 shows the  $10\sigma$  profiles of the beam in the horizontal and vertical planes. They have been calculated using both methods discussed earlier. The orbits agree all along the beam line, showing that the tracking methods are equivalent.

All the results presented in this paper have been obtained with a program which simulates particle trajectories using the beam optics transport equation (4). This program reflects in its main features the TRANSPORT beam optics program [11] and is similar to the simulation program used to design the Leading Proton Spectrometer at ZEUS [5, 12]. The beta value at the intersection point considered in the calculation is 1000 m.

A short description of the main characteristics of the simulation program is given in the following. Given the beam momentum, a track is followed from the starting point until it is lost at an obstruction. The program returns the hit pattern at selected positions where detectors may be placed. The elements along the beam line which have been simulated are:

- Drifts - in which no particle is lost and which have the same aperture as that of the previous element.
- Quadrupoles - the focussing effect is calculated as a function of  $x_L$ . Negative focal length means horizontal focussing. Negative  $x_L$  means particle with negative charge.

- Dipoles - the bending power is calculated with respect to that for a track at  $x_L = 1$ , so that no bending occurs for particles at  $x_L = 1$ . During tracking inside a magnetic element the distance of the particle from the nominal beam may reach a local maximum and a test is done to see if this maximum is outside the beam pipe. The same test is performed at the entrance and at the exit of each quadrupole.
- Detectors - at present these are considered to be virtual planes covering the whole beam pipe aperture except for a rectangular hole with sides of length equal to  $10\sigma_x$  and  $10\sigma_y$ , where  $\sigma_x$  and  $\sigma_y$  are the horizontal and vertical standard deviation of the beam distribution (taken to be a Gaussian), respectively.

For the following study particles were generated in the interaction vertex diamond of dimensions  $(\Delta x, \Delta y, \Delta z) = (0.6\text{mm}, 0.6\text{mm}, 0.0\text{mm})$ , according to a flat distribution in  $\log(1 - x_L)$  within the limits  $10^{-4} < (1 - x_L) < 10^{-1}$  and a flat distribution in  $\log(p_T)$  within the limits  $10^{-4} < p_T < 1 \text{ MeV}/c$ . The  $z$  axis points in the proton beam direction. The  $x_L$  distribution has been chosen because it reflects the observed single diffractive cross section, the  $p_T$  distribution in order to enhance the generation of particles at very low  $p_T$  (and thus at very low  $|t|$ ) and therefore approach the optical point ( $t = 0$ ) in the study of the elastic cross section at  $(1 - x_L) = 0$ .

### 3 The spectrometers

In order to maximize the geometric acceptance all the detectors are placed in the region beyond 200 m from the IP where the beam profile has the smallest transverse size (see Fig.3).

In this way we select three regions where the beam elements can be used to momentum analyse very forward outgoing protons. We call them spectrometers  $A$ ,  $B$ ,  $C$ . Each of them consists of two detector planes positioned upstream and downstream of a dipole element. The detector planes are located only where the distance between adjacent magnetic elements is  $\gtrsim 50 \text{ cm}$ .

Fig.4 shows particle trajectories through one of the outgoing arms from IP4. They are calculated considering two values of  $x_L$  and three values of  $p_T$ . We choose two extreme  $p_T$  values of  $\pm 2 \text{ GeV}/c$  and the central value  $p_T = 0$ . The beam pipe diameter has been taken to be infinite when tracking particles at this stage. Vertical bands are superimposed to indicate the positions of the three spectrometers.

Table 4 summarizes the positions and characteristics of the planes of each of the spectrometers.

In addition to spectrometers  $A$ ,  $B$ ,  $C$  which cover the *very forward* region, there is a 45 m long drift space downstream of the central experimental region between dipoles  $D1$  and  $D2$  which allows the detection of the forward going leading particles with low  $x_L$  down

to  $x_L \sim 0$ . The geometrical acceptance is calculated also for this region in order to see which range of  $x_L$  and  $p_T$  can be detected outside the vacuum beam pipe. A preliminary study of this region is given in [7].

## 4 Geometrical acceptance and momentum resolution

At least three points are needed to measure the momentum. We use the interaction vertex and demand the coincidence of any two detector planes (double coincidence events). Using the transport matrix (4) we relate the impact point of the track on the detector to the position and angle of the track at the interaction point. At plane  $i$  we can write the equation

$$x_i = H_{i,11} x(0) + H_{i,12} \theta_x(0). \quad (5)$$

Assuming the nominal vertex ( $x(0)=0$ ) we can also relate the position of the track at two different planes  $i, j$  with the equation

$$x_i = M_{ij}(x_L) x_j + C_{ij}(x_L). \quad (6)$$

For a given pair of detectors  $i, j$  and for a given value of  $x_L$ , the coordinates  $x_i$  and  $x_j$  are thus linearly correlated; the parameters of the straight line are functions of  $x_L$  only, thereby allowing the determination of  $x_L$  from double coincidence events.

This method is used for momentum reconstruction in the ZEUS LPS [5] and a longitudinal momentum resolution of 0.4% has been achieved for particles at  $x_L = 1$ ; the resolution on the transverse plane for the ZEUS LPS is less than the beam transverse momentum spread of  $\sim 40 - 100$  MeV/c.

Fig.5 shows the pattern of hits at the detector planes of the three spectrometers. The  $10\sigma$  profile of the beam is often clearly visible. The area covered by the hits on each plane is always asymmetric. This asymmetry originates from the bending and focalizing power of all the magnetic elements of the proton beam line upstream of the detector planes; this must be taken into account in order to define the best geometry of the detector planes.

Fig.6 shows the correlation between horizontal and vertical coordinates for the different pairs of detector planes which are used to calculate the momentum. The regions of the planes which detect very high  $x_L$  and very small  $p_T$  tracks correspond, in the figure, to the areas of higher event density. This is because of the particular generation we have used which is mentioned in the previous section. The straight lines, superimposed to the scatter plot shown in Fig.6c, correspond to the different values of  $x_L$  at which particles were generated. Correlations on the horizontal plane provide a good  $x_L$  resolution because the lines which represent two adjacent values of  $x_L$  are well separated. On the other hand on the vertical plane the lines representing the same values of  $x_L$  would be densely packed and are not used for resolution calculation.

The geometric acceptance for the double coincidence events is shown in Fig.7, Fig.8 and Fig.9 as a function of  $\xi$  and  $p_T$  for the spectrometers  $A$ ,  $B$  and  $C$ , respectively. The acceptance is limited by the vacuum beam pipe apertures at the highest values of  $\xi$  and the highest values of  $p_T$ . On the other hand particles with very small  $p_T$  and with momentum close to the beam momentum escape within the  $10\sigma$  detector apertures.

From Fig.7, Fig.8 and Fig.9 we can conclude that spectrometer  $A$  has 100% acceptance in the region  $0.03 \lesssim \xi \lesssim 0.1$  and  $1 \lesssim p_T \lesssim 10^3$  MeV/c and in the region  $10^{-4} \lesssim \xi \lesssim 0.1$  and  $10^2 \lesssim p_T \lesssim 10^3$  MeV/c. Spectrometer  $B$  has 100% acceptance in the region  $10^{-2} \lesssim \xi \lesssim 0.03$  and  $1 \lesssim p_T \lesssim 10^3$  MeV/c and in the region  $10^{-4} \lesssim \xi \lesssim 0.03$  and  $50 \lesssim p_T \lesssim 500$  MeV/c. Finally spectrometer  $C$  has 100% acceptance in the region  $10^{-3} \lesssim \xi \lesssim 10^{-2}$  and  $1 \lesssim p_T \lesssim 10^3$  MeV/c. In general very low  $\xi$  tracks are accepted for  $10^2 \lesssim p_T \lesssim 10^3$  MeV/c, and very low  $p_T$  tracks are accepted in the region  $10^{-3} \lesssim \xi \lesssim 0.1$ .

A different region of  $\xi$  can be studied by a spectrometer placed in the 45 m long drift region between dipoles D1 and D2. Two detector planes have been assumed at the beginning and at the end of this drift space and their geometrical acceptance is shown in Fig.10 as a function of  $\xi$  and  $p_T$ . In this case  $\xi$  has been generated uniformly between 0 and 1. The figure shows a wide interval of  $\xi$  between 0.15 and 0.6 in which the acceptance at the beginning of the drift space is 100% for particles inside the pipe. The acceptance does not depend on  $p_T$ . At the end of the drift space only particles with  $\xi \lesssim 0.2$  stay inside the beam pipe and, if we require the coincidence of the two planes, particles are accepted only in a very limited region of  $\xi$ . This means that particles with  $0.2 \lesssim \xi \lesssim 0.6$  can be analysed with detectors (and magnets) placed outside the vacuum pipe.

The momentum resolution  $\frac{\Delta x_L}{x_L}$  has been calculated for the three spectrometers with either  $100\mu\text{m}$  or  $10\mu\text{m}$  pitch detectors and is shown in Fig.11. Two different sets of curves are shown in the figure. The continuous lines show the momentum resolution for the three spectrometers  $A, B, C$  equipped with  $100\mu\text{m}$  pitch detectors, while the dashed lines show the resolutions for  $10\mu\text{m}$  pitch detectors. All curves show an approximately constant behaviour in the considered  $(1 - x_L)$  interval, and in general the spectrometers with  $10\mu\text{m}$  pitch detectors show a resolution which is one order of magnitude better than the stations with  $100\mu\text{m}$  pitch detectors. The resolution improves as the distance from the interaction point increases. This effect originates from the increased integrated magnetic field acting on the particle. The best resolution is obtained with spectrometer C and has the values  $\frac{\Delta x_L}{x_L} \sim 10^{-3}\%$  and  $\frac{\Delta x_L}{x_L} \sim 10^{-4}\%$  for the  $100\mu\text{m}$  and  $10\mu\text{m}$  pitch detectors, respectively. Spectrometer C accepts however only particles with  $(1 - x_L) \lesssim 10^{-2}$  due to the large distance of the detectors from the interaction point. We can conclude that the order of magnitude of the momentum resolution is always better of 1 GeV/c for a typical momentum of  $7 \cdot 10^3$  GeV/c.

The momentum resolution calculated using vertical coordinate correlations is very poor compared to the previous one. This can be seen also from Fig.6 where the vertical correlation lines are very densely packed and generate many ambiguities in the momentum calculation.

The transverse momentum resolution  $\frac{\Delta p_T}{p_T} = \frac{(p_T(rec) - p_T(gen))}{p_T(gen)}$  as a function of  $p_T(gen)$  has been studied for the three spectrometers separately, with either  $100\mu\text{m}$  or  $10\mu\text{m}$  pitch detectors.

The transverse momentum  $p_T$  has been calculated using the two components  $p_x$  and  $p_y$  computed using the relation:

$$p_x(0) = \theta_x(0) x_L(hor) p_{beam}, \quad (7)$$

where  $\theta_x(0)$  is obtained from the transport matrix eq.(4), and  $x_L(hor)$  is the momentum estimate in the horizontal plane. The  $p_y$  component is calculated using a similar equation in the  $y$  plane, but still considering the momentum estimate  $x_L(hor)$ .

Fig.12 shows the  $p_T$  resolution for spectrometer A for two different detector pitches. We can observe that the resolution is always better than 3% for  $p_T \gtrsim 200$  MeV/c and slowly improves as a function of  $p_T$ . No  $x_L$  dependence is observed both in the case of  $100\mu\text{m}$  and  $10\mu\text{m}$  pitch detectors. The resolution is a factor of two better for the  $10\mu\text{m}$  pitch detectors planes in all  $p_T$  bins considered. The best resolution in spectrometer A is of the order of 0.1%. Fig.13 shows the  $p_T$  resolution for the spectrometers B and C. Full and open symbols represent the resolution for the  $100\mu\text{m}$  and for the  $10\mu\text{m}$  pitch detectors, respectively. In all cases the resolution slowly improves as a function of  $p_T$  and takes values which are approximately of the same order of magnitude as those observed in spectrometer A. Finally it is interesting to notice that the calculated resolution in the whole  $p_T$  range considered is of the order of the nominal beam transverse momentum spread ( $\lesssim 5$  MeV/c).

## 5 Conclusions

Geometrical acceptance and momentum resolution have been calculated for three spectrometers along one of the outgoing proton beam arms of IP4 at LHC in the interval  $10^{-4} \lesssim \xi \lesssim 0.1$  and  $0 \lesssim p_T \lesssim 10^3$  MeV/c. The apparatus has been simulated with  $100\mu\text{m}$  or with  $10\mu\text{m}$  pitch detector planes. We have shown that the three spectrometers cover regions of  $x_L$  which partially overlap. They have very different momentum resolutions for equal values of  $x_L$  but their  $p_T$  resolution do not differ dramatically. In general going from  $100\mu\text{m}$  to  $10\mu\text{m}$  pitch an order of magnitude in the momentum resolution is gained, while only a factor two is gained for the  $p_T$  resolution. The momentum resolution is in the range  $10^{-4}\% \lesssim \frac{\Delta x_L}{x_L} \lesssim 5 \cdot 10^{-2}\%$ . The  $p_T$  resolution is in the range  $0.1\% \lesssim \frac{\Delta p_T}{p_T} \lesssim 3\%$  for particles with  $p_T \gtrsim 200$  MeV/c.

## Acknowledgments

The results presented in this paper were obtained in the early stages of the effort that recently led to the completion of the FELIX Letter of Intent [13]. We are grateful to the authors of [8] for many discussions. In particular we are indebted to K. Eggert and A. Morsch for their interest in our work, for many useful suggestions and for carefully reading the manuscript.

## References

- [1] See e.g.:
- T.Regge, *Nuovo Cimento* 14 (1959) 951;
  - G.F.Chew, S.C. Frautschi, *Phys., Rev. Lett.* 7 (1961) 394;
  - A.H.Mueller, *Phys Rev.* D2 (1970) 2963;
  - F.E.Low, *Phys. Rev.* D12 (1975) 163;
  - S. Nussinov, *Phys. Rev.* D14 (1976) 246;
  - U. Amaldi, M. Jacob and G. Matthiae, *Ann. Rev. Nucl. Sci.* 26 (1976) 385;
  - P.D.B. Collins, “An Introduction to Regge Theory and High Energy Physics”, Cambridge University Press, Cambridge, 1977;
  - A.B. Kaidalov, *Phys. Rep.* 50 (1979) 157;
  - G.Alberi and G. Goggi, *Phys. Rep.*74 (1981) 1;
  - K. Goulianos, *Phys. Rep.* 101 (1983) 169;
  - L.V. Gribov, E.M. Levin and M.G. Ryskin, *Phys. Rep.* 100 (1983) 1;
  - N.Arteaga-Romero et al., *Mod. Phys. Lett.* A1 (1986) 221;
  - G. Ingelman, P. Schlein, *Phys. Lett.* 152B (1985) 256;
  - A. Donnachie, P.V. Landshoff, *Nucl. Phys. B* 303 (1988) 634;
  - N.N.Nikolaev, B.G.Zakharov, *Z. Phys.* C49 (1991) 607;
  - J.D. Bjorken, SSC EOI 19, *Int. J. Mod.Phys.* A7 (1992) 4189.
- [2] U.Amaldi et al., *Phys. Lett. B* 43 (1973) 231.
- [3] See e.g.:
- Y.Akimov et al., *Phys. Rev.* D14 (1976) 3148;
  - M.G. Albrow et al., *Nucl. Phys. B* 108 (1976) 1;
  - R.L.Cool et al., *Phys. Rev. Lett.* 47 (1981) 701;
  - M.Bozzo et al., UA4 Collaboration, *Phys. Lett.* 136B (1984) 217;
  - M. Bozzo et al., *Phys. Lett. B* 136 (1984) 217;
  - K.Eggert, UA1 Collaboration, *Proceedings of the Int. Conference on Elastic and Diffractive Scattering 15-18 Oct.1987*, Ed. K.Goulianos, The Rockefeller Univ., New York, p.1;
  - R. Bonino et al., UA8 Collaboration, *Phys. Lett. B* 211 (1988) 239;
  - A.Brandt et al., UA8 Collaboration, *Phys. Lett. B* 297 (1992) 417.
- [4] See e.g.:
- ZEUS Collaboration, M. Derrick et al., *Z. Phys.* C68 (1995) 569;



- H1 Collaboration, T. Ahmed et al., Phys. Lett. B348 (1995) 681;  
H1 Collaboration, T. Ahmed et al., Nucl. Phys. B435 (1995) 3;  
ZEUS Collaboration, M. Derrick et al., Phys. Lett. B346 (1995) 399;  
ZEUS Collaboration, M. Derrick et al., Phys. Lett. B350 (1995) 120;  
ZEUS Collaboration, M. Derrick et al., Phys. Lett. B356 (1995) 129;  
ZEUS Collaboration, M. Derrick et al., Z. Phys. C69 (1995) 39;  
ZEUS Collaboration, M. Derrick et al., Z. Phys. C70 (1996) 391;  
H1 Collaboration, T. Ahmed et al., Z. Phys. C70 (1996) 609;  
H1 Collaboration, T. Ahmed et al., Nucl. Phys. B472 (1996) 32;  
ZEUS Collaboration, M. Derrick et al., Phys. Lett. B380 (1996) 220;  
ZEUS Collaboration, M. Derrick et al., Z. Phys. C73 (1996) 73.
- [5] ZEUS Collaboration, "The ZEUS Detector, Status Report 1993", PRC/93;  
ZEUS Collaboration, M. Derrick et al., accepted by Z. Phys. C73 (1997) 253.
- [6] G. Matthiae, Proceedings Large Hadron Collider Workshop CERN 90-10, Vol 2;  
TOTEM Collaboration, M.Bozzo et al., EOI CERN/LHCC 93-47;  
K. Eggert and A. Morsch, CERN AT/94-09;  
K. Eggert and A. Morsch, Nucl. Instr. and Meth. A351 (1994) 174.
- [7] T. Taylor, H.Wenninger and A. Zichichi, CERN-LAA/95-15.
- [8] Y. Takahashi et al., CERN/LHCC 95-51 (LHC);  
K. Eggert, A. Morsch and C. Taylor "A full acceptance experiment at the CERN Large Hadron Collider (LHC)" , VII th Blois workshop on Elastic and Diffractive Scattering, June 1995 published in Frontiers in Strong Interactions (1995), editors P. Chiapetta, M.Haguenaue and J. Tran Thanh Van;  
K. Eggert and C. Taylor, "FELIX, A Full Acceptance Detector for the CERN LHC", Nucl. Phys. B (Proc. Suppl.) 52B (1997) 279.
- [9] S. Maselli, "A small angle spectrometer for very forward physics at LHC" Proceedings of the Sixth Topical Seminar on Experimental Apparatus for Particle Physics and Astrophysics, S.Miniato, 20-24 May 1996, Nucl. Phys. B54 (1997) 74.
- [10] The LHC Study Group, CERN/AC/95-05 (LHC).
- [11] K.L.Brown et al., CERN Yellow Report 80-04.
- [12] T. Massam, BEAM9, a program to simulate the Leading Proton Spectrometer at ZEUS, 1992 (unpublished).

At the time of printing the following references became available:

- [13] FELIX, “A full acceptance detector at the LHC”, Letter-of-Intent LHCC/I10, CERN/LHCC 97-45, 1st Aug. 1997.
- [14] A. Verdier, “A tunable insertion in point 4 for LHC” LHC Project Note 93, June 1997.

Name	Type	start [m]	length [m]	spot considered [mm] x [mm]	parameter [mrad] if bend [m] if quad
LALEPH	drift	0.	3.83	-	
DUA1	bend	3.83	4.95	-	0.170
L2	drift	8.78	2.72	-	
D0	bend	11.5	2.0	-	0.342
L3	drift	13.5	4.5	-	
D1	bend	18.0	9.45	44 x 44	1.62
L4	drift	27.45	0.6		
D1	bend	28.05	9.45	44 x 44	1.62
L5	drift	37.5	45.265		
D2	bend	82.765	9.45	44 x 44	-1.62
L6	drift	92.215	0.6		
D2	bend	92.815	9.45	44 x 44	-1.62
L7	drift	102.265	2.2		
Q1	quad	104.465	5.5	35 x 35	74.822
L8	drift	109.965	4.5		
Q2	quad	114.465	5.5	35 x 35	-52.397
L9	drift	119.965	1.0		
Q2	quad	120.965	5.5	35 x 35	-52.397
L10	drift	126.465	5.5		
Q3	quad	131.965	5.5	35 x 35	39.440
L11	drift	137.465	1.8		

Table 1: Positions of the beam elements of one of the two outgoing proton beams with respect to the IP4 and the corresponding field values considered in the simulation program. The spot considered is the area transverse to the nominal beam available for the passage of particles.

Name	Type	start [m]	length [m]	spot considered [mm] x [mm]	parameter [mrad] if bend [m] if quad
L12	RF cav	139.265	33.528		
Q4	quad	172.793	3.0	28 x 28	-123.001
L13	drift	175.793	20.0		
Q5	quad	195.793	3.0	28 x 28	85.251
L14	drift	198.793	1.2		
D3	bend	199.993	9.45	38 x.38	-1.62
L15	drift	209.443	0.6		
D3	bend	210.043	9.45	38 x.38	-1.62
L16	drift	219.493	16.0		
D4	bend	235.493	9.45	38 x.38	1.62
L17	drift	244.943	0.6		
D4	bend	245.543	9.45	38 x.38	1.62
L18	drift	254.993	1.0		
L19	drift	255.993	0.2		
Q6	quad	256.193	3.0	28 x 28	-45.045
L20	drift	259.193	0.2		
Q6	quad	259.393	3.0	28 x 28	-45.045
L21	drift	262.393	2.5		
BDS0	bend	264.893	14.2		5.1
L22	drift	279.093	1.46		
BDS0	bend	280.553	14.2		5.1
L23	drift	294.753	2.14		
Q7	quad	296.893	3.25	22 x 18	34.150
L24	drift	300.143	0.2		
Q7	quad	300.343	1.5	22 x 18	1536.098

Table 2: Same as Table 1.

Name	Type	start [m]	length [m]	spot considered [mm]	parameter [mrad] if bend [m] if quad
L25	drift	301.843	8.91		
BDS0	bend	310.753	14.2		5.1
L26	drift	324.953	1.46		
BDS0	bend	326.413	14.2		5.1
L27	drift	340.613	2.14		
Q8	quad	342.753	3.25	22 x 18	-34.150
L28	drift	346.003	0.2		
Q8	quad	346.203	1.5	22 x 18	-139.762
L29	drift	347.703	4.86		
BDS0	bend	352.563	14.2		5.1
L30	drift	366.763	1.46		
BDS0	bend	368.233	14.2		5.1
L31	drift	382.423	2.14		
Q9	quad	384.563	3.25	22 x 18	34.150
L32	drift	387.813	0.2		
Q9	quad	388.013	1.5	22 x 18	175.438
L33	drift	389.513	4.99		
BDS0	bend	394.503	14.2		5.1
L34	drift	408.703	1.46		
BDS0	bend	410.200	14.2		5.1
L35	drift	424.363	9.321		
Q10	quad	433.684	1.5	22 x 18	-959.233
L36	drift	435.184	0.2		
Q10	quad	435.384	1.5	22 x 18	-73.992

Table 3: Same as Table 1.

<b>Spectrometer A</b>			
Detectors	Position [m]	$\sigma_x$ of beam [mm]	$\sigma_y$ of beam [mm]
A1	175.793	0.50	0.27
A2	219.493	0.37	0.01
<b>Spectrometer B</b>			
Detectors	Position [m]	$\sigma_x$ of beam [mm]	$\sigma_y$ of beam [mm]
B1	301.843	0.17	0.06
B2	340.613	0.04	0.04
<b>Spectrometer C</b>			
Detectors	Position [m]	$\sigma_x$ of beam [mm]	$\sigma_y$ of beam [mm]
C1	389.513	0.23	0.09
C2	424.363	0.13	0.21

Table 4: List of detector planes considered in the three spectrometers and  $1\sigma$  beam sizes at the planes.

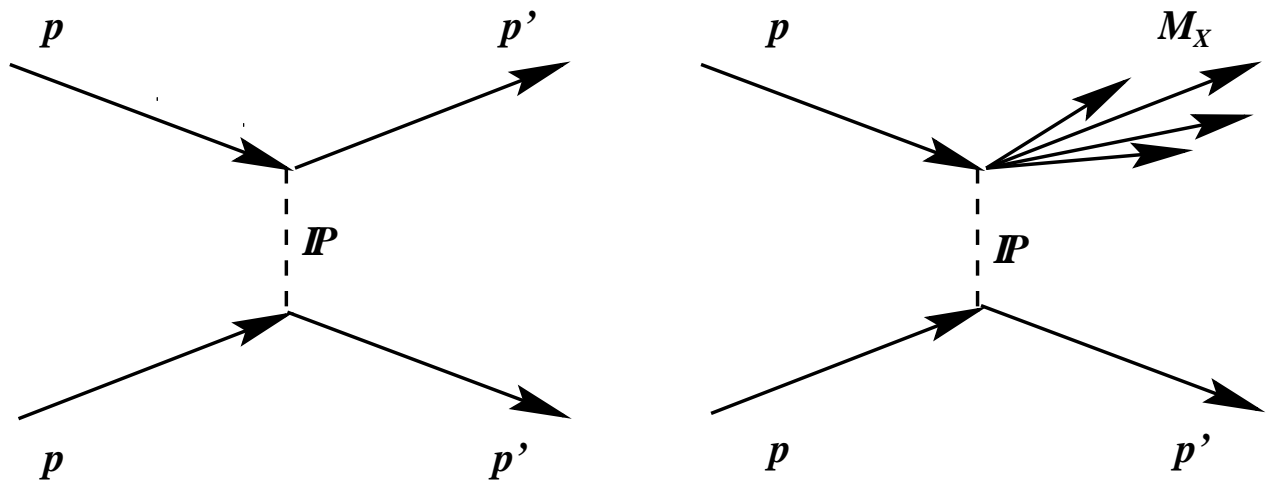


Figure 1: Single pomeron ( $\mathbb{P}$ ) exchange in elastic (a) and single diffractive (b)  $pp$  interactions. In interactions of type (b) a final hadronic system  $M_X$  is produced.

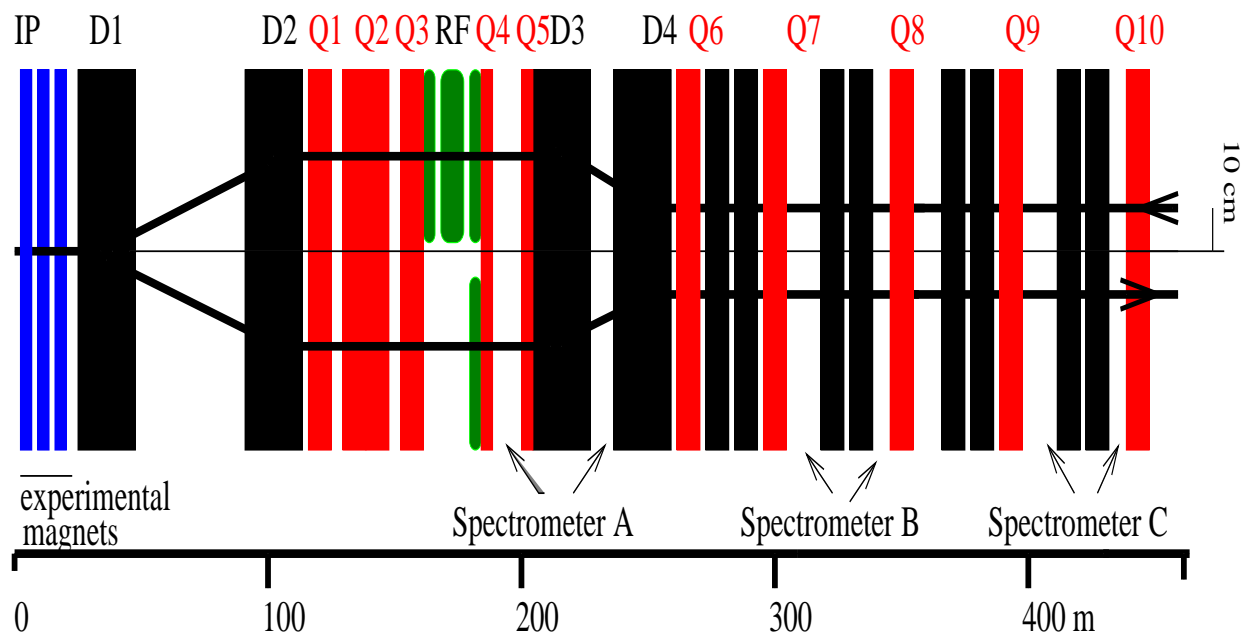


Figure 2: Plan view of a possible insertion in IP4 showing the positions of the three spectrometers considered in this paper (from [8]).



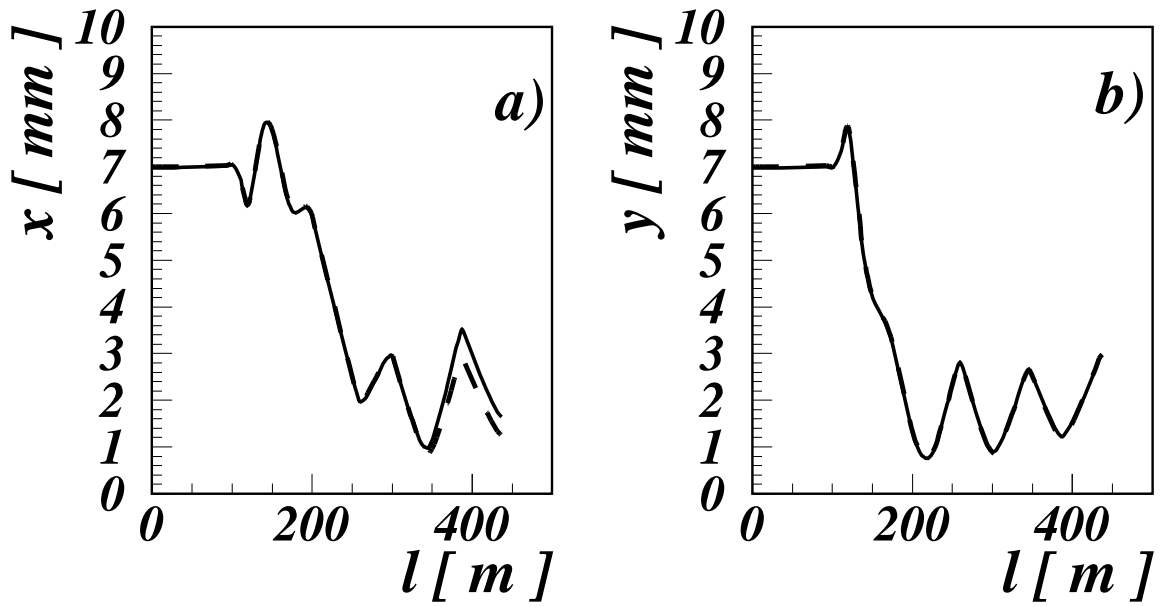


Figure 3:  $10\sigma$  profiles a) horizontal; b) vertical. The continuous lines show the orbits calculated with eqs.(1),(2) (as in [8]) the dashed lines those calculated with eq.(4).

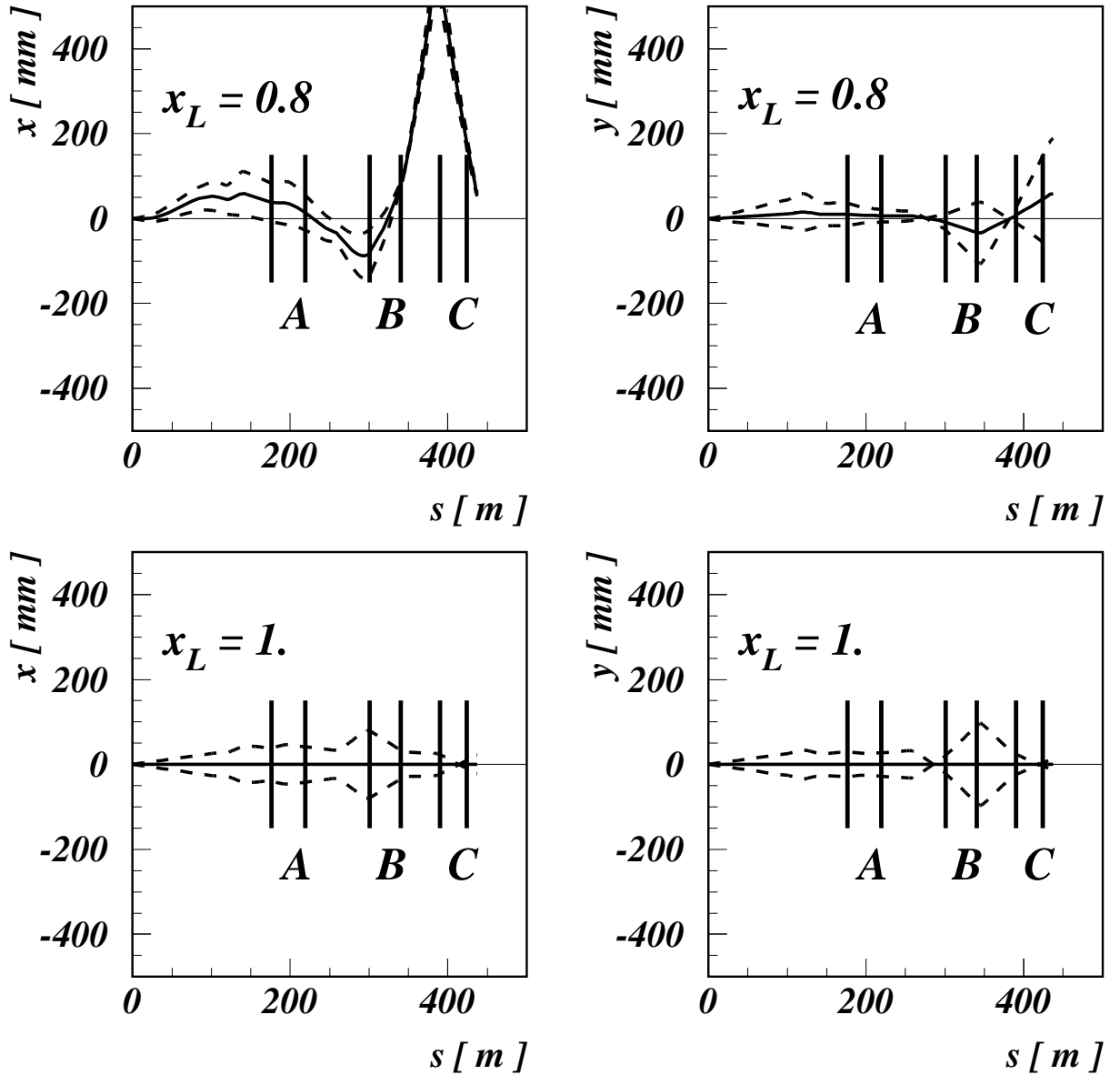


Figure 4: Typical horizontal and vertical trajectories of particles through the magnetic elements of the beam line at different  $x_L$  and  $p_T$  values. The continuous lines correspond to particles with  $p_T = 0$ , the two dashed lines correspond to particles with  $p_T = \pm 2$  GeV/c.

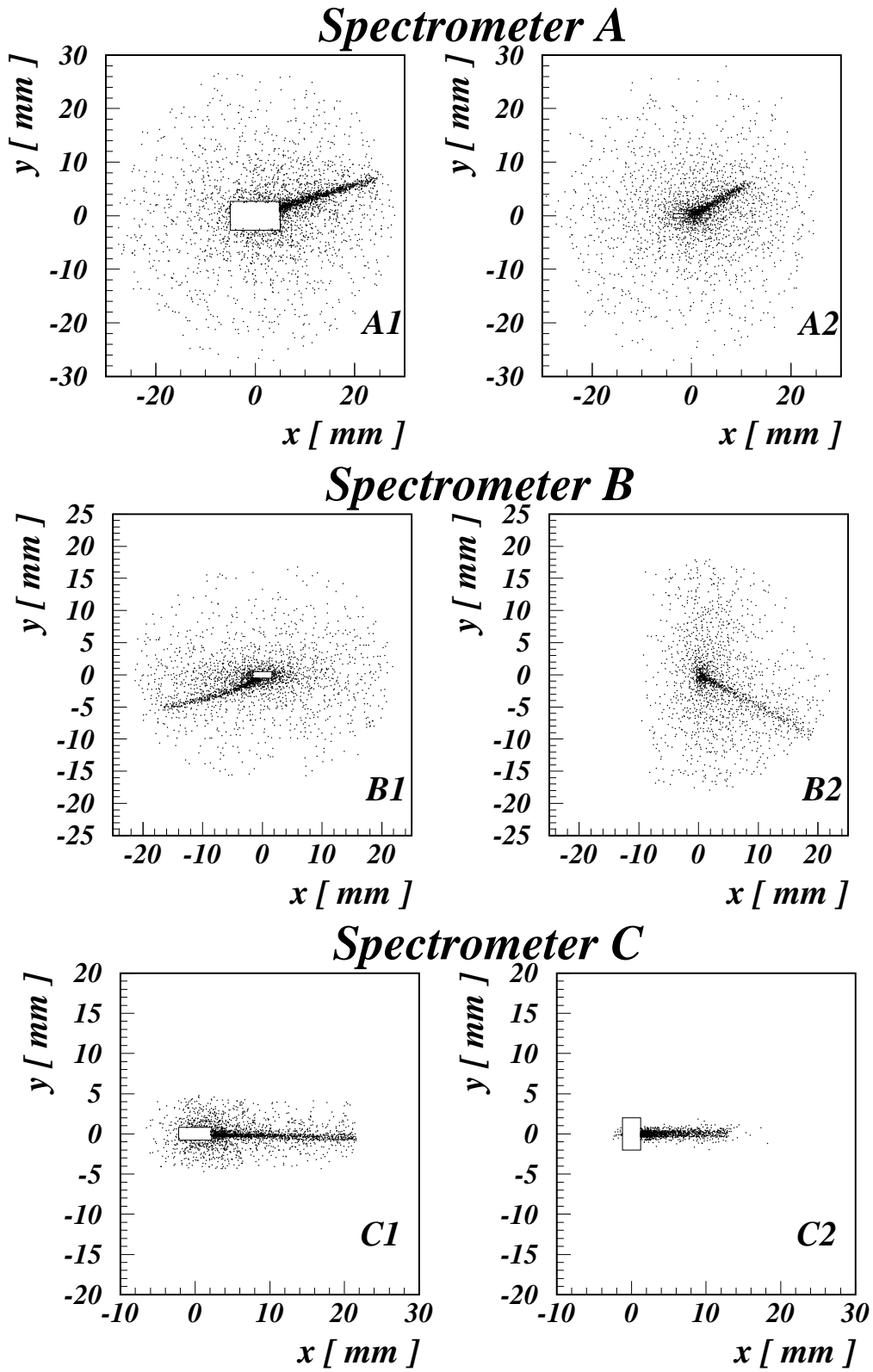


Figure 5: Distribution of the hits at the detector planes of spectrometers A, B and C. A box is drawn at each plane representing the dimensions of the  $10\sigma$  profile of the beam.

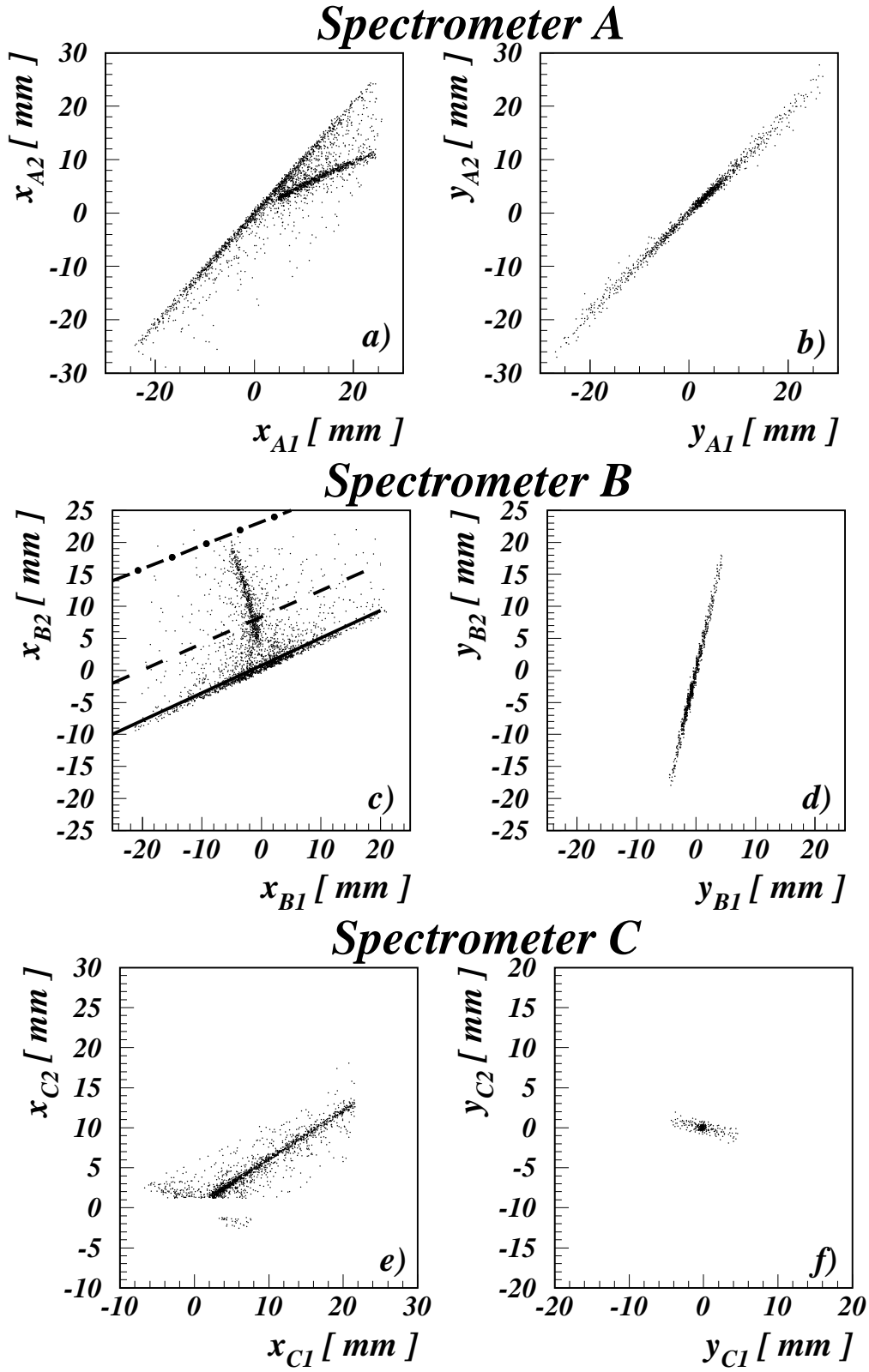


Figure 6: Correlations between track positions in pairs of planes of the spectrometers. Continuous, dashed, dot-dashed lines in (c) correspond to tracks with  $x_L = 0.999, x_L = 0.980, x_L = 0.945$ , respectively.

# *Spectrometer A*

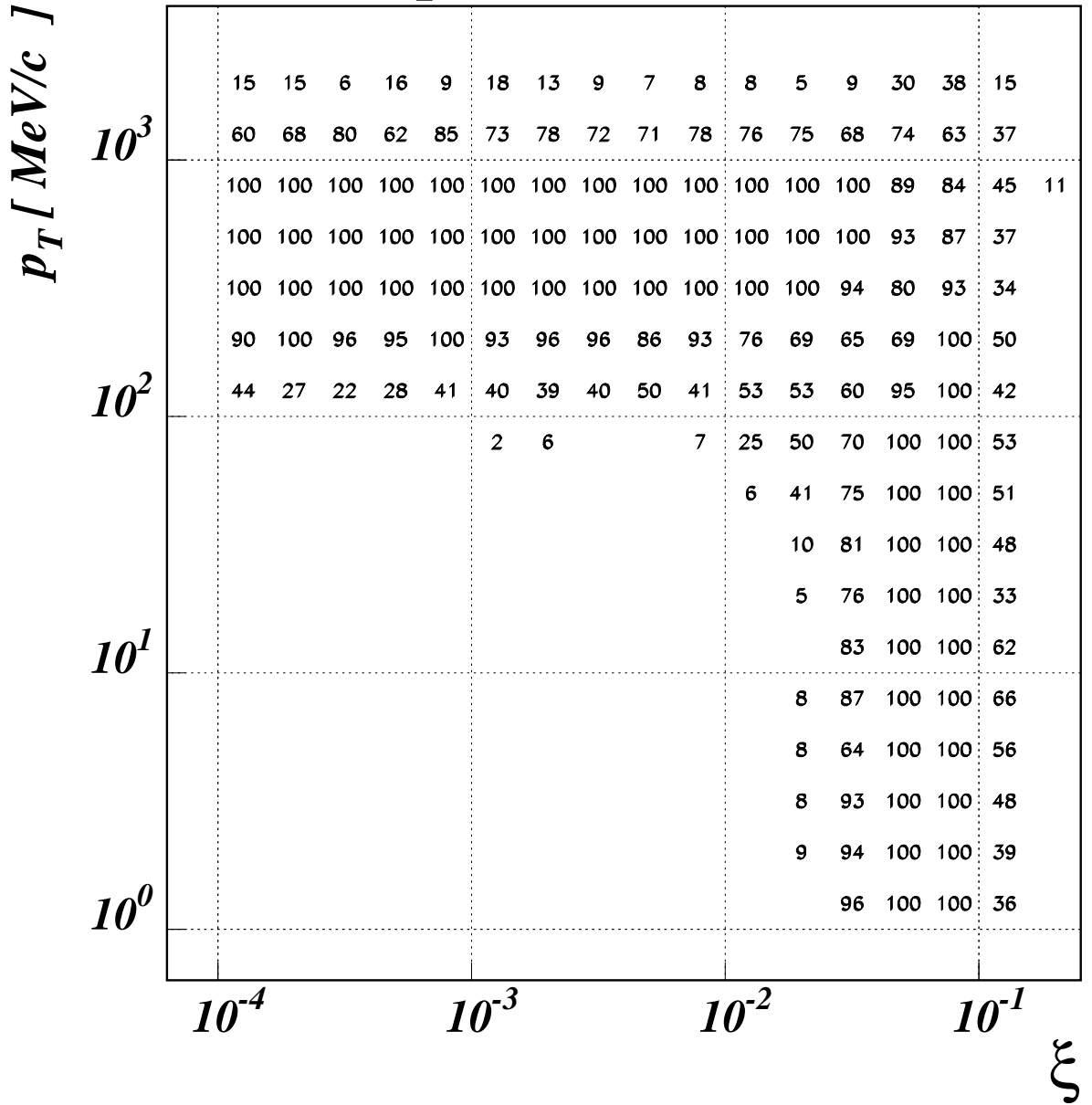


Figure 7: Geometrical acceptance as a function of  $\xi$  and  $p_T$  for double coincidence events in spectrometer A.

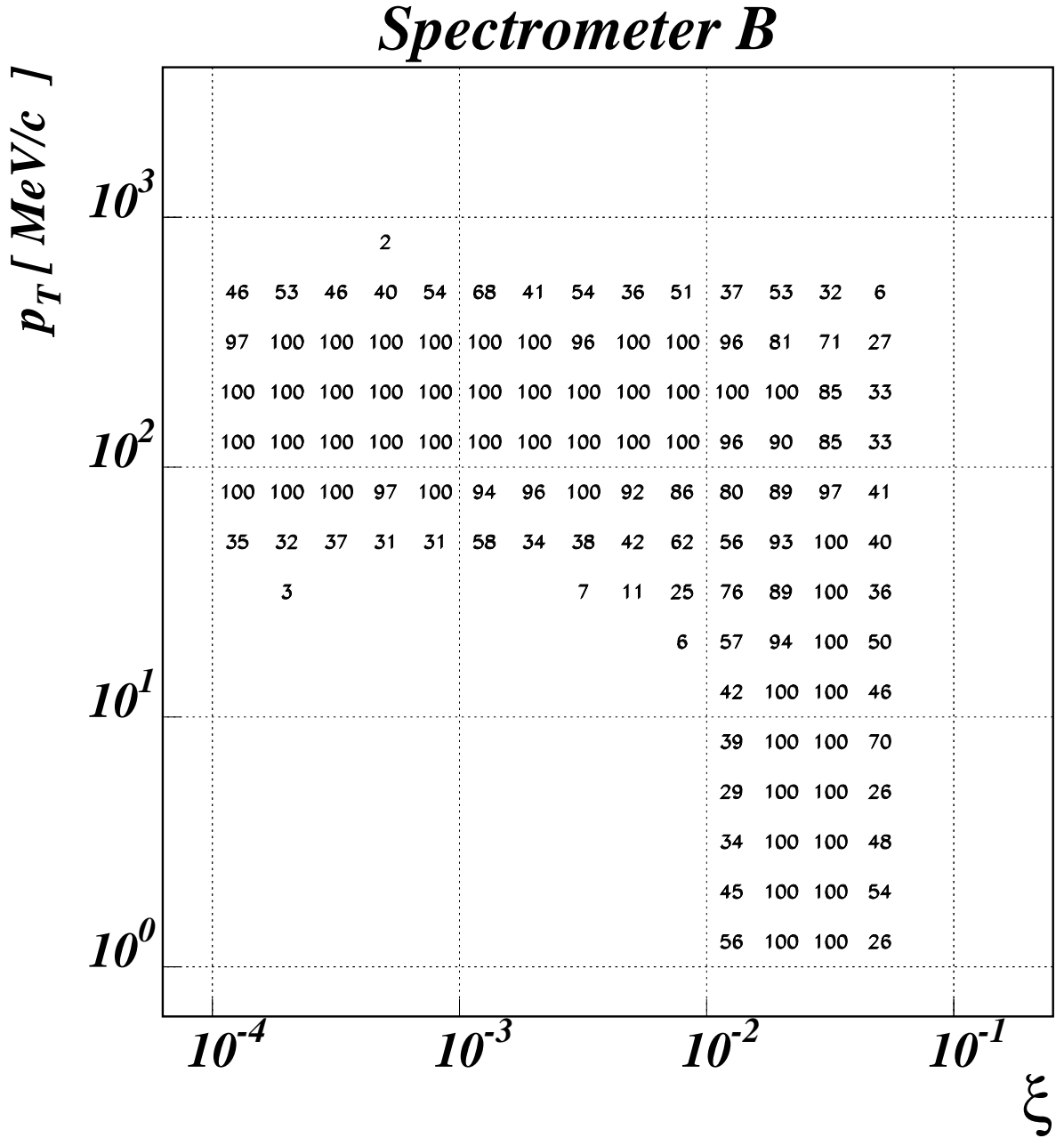


Figure 8: Geometrical acceptance as a function of  $\xi$  and  $p_T$  for double coincidence events in spectrometer *B*.

## *Spectrometer C*

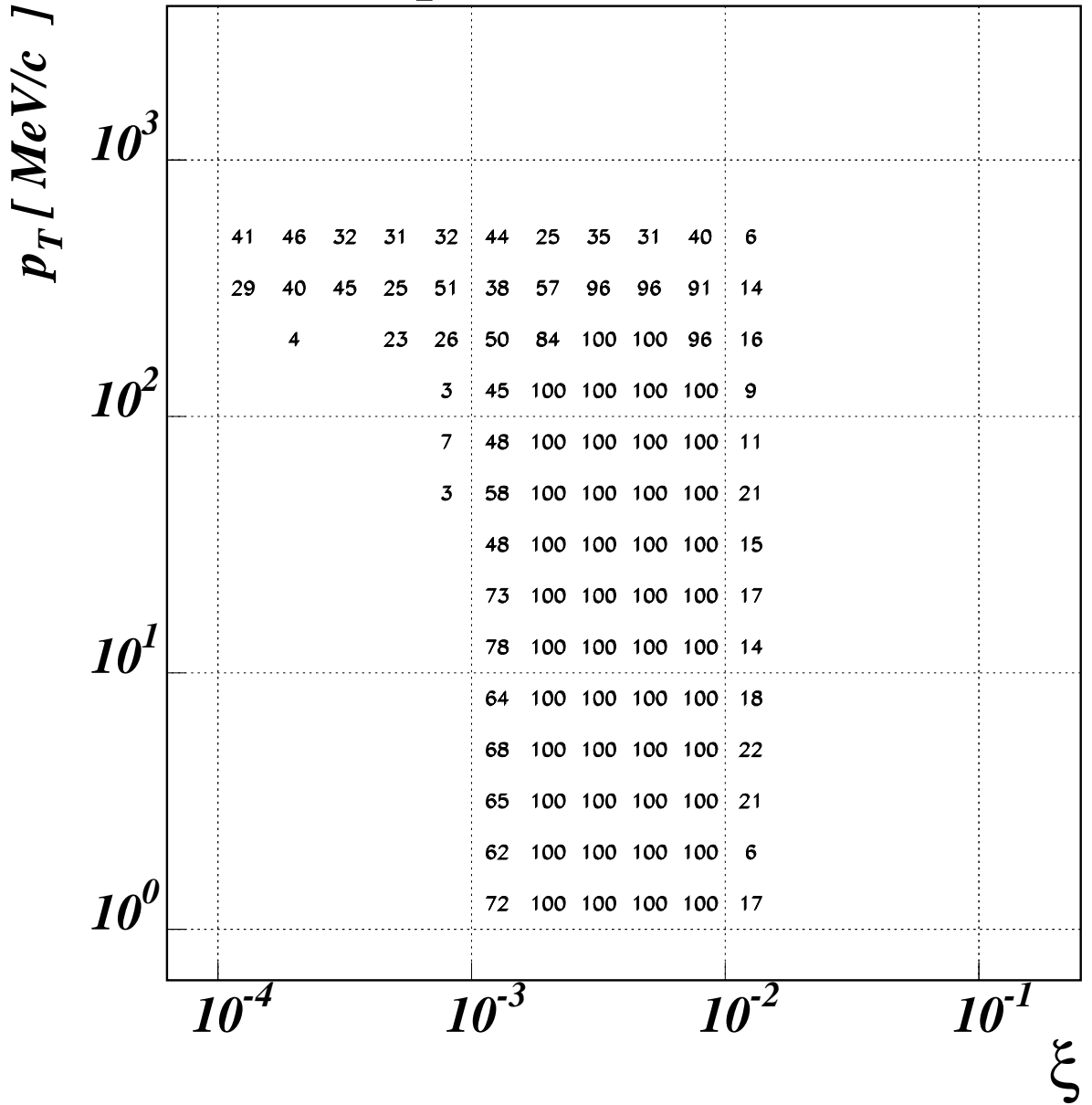


Figure 9: Geometrical acceptance as a function of  $\xi$  and  $p_T$  for double coincidence events in spectrometer *C*.

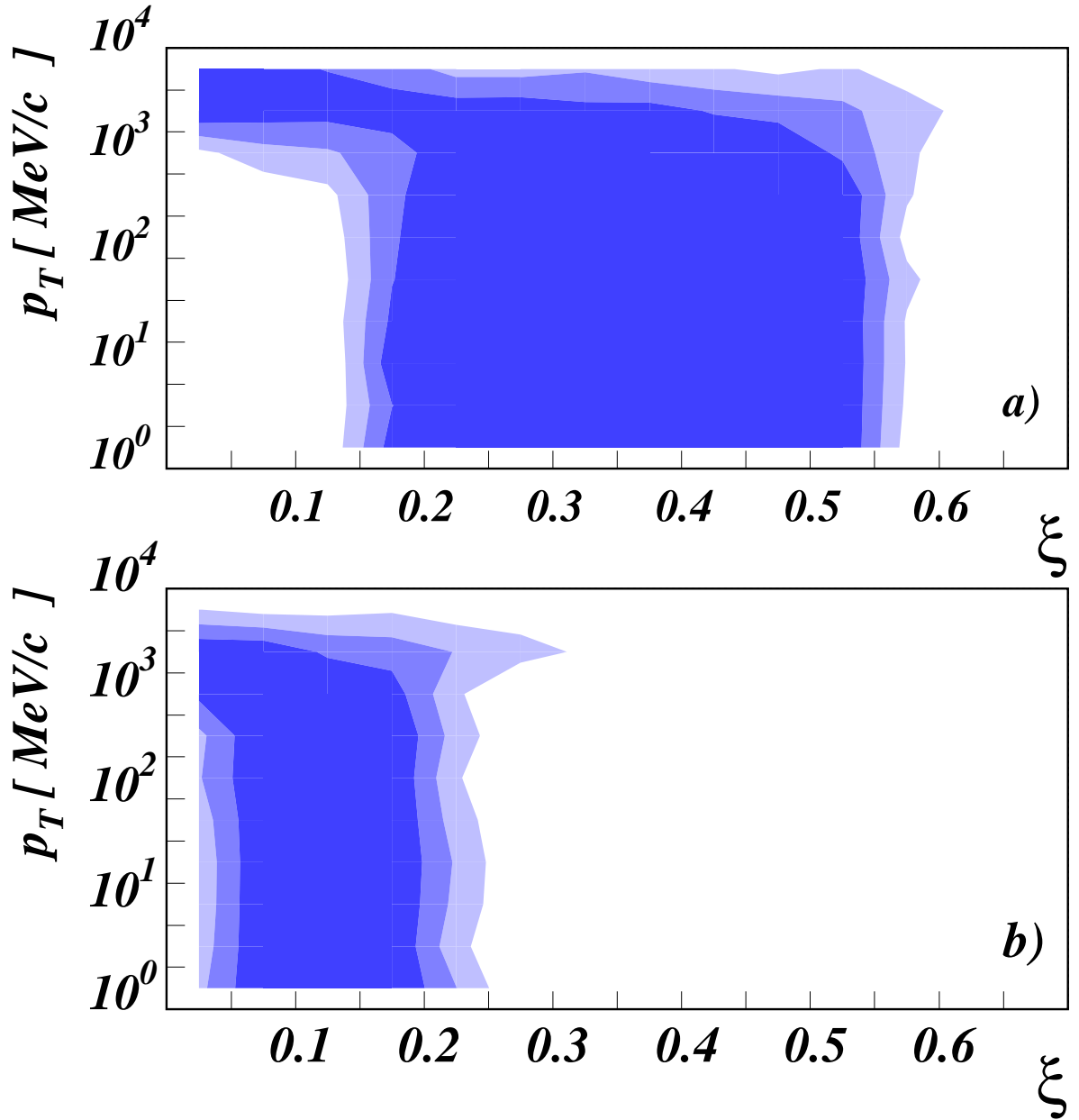


Figure 10: Geometric acceptance as a function of  $\xi$  and  $p_T$  for two planes placed at the beginning (a) and at the end (b) of the 45 m drift space between dipoles D1 and D2. Three acceptance ranges are shown in the pictures:  $\sim 100\%$  (dark grey), 100 – 50%, and 50 – 0% (light grey).



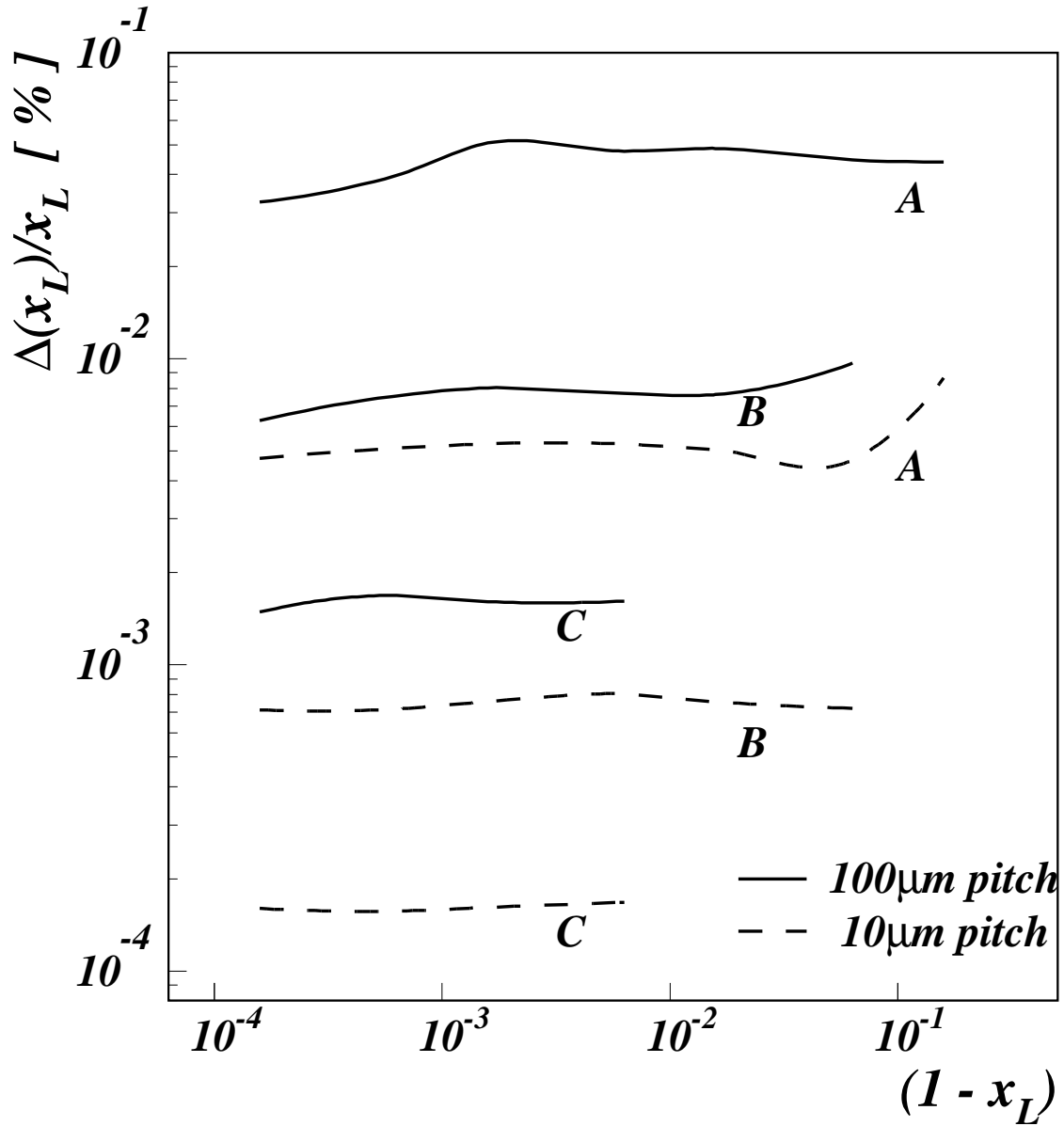


Figure 11: Momentum resolution  $\frac{\Delta x_L}{x_L}$  for the spectrometers A, B and C. Results for  $100\mu\text{m}$  (continuous lines) and  $10\mu\text{m}$  (dashed lines) pitch detectors are shown.

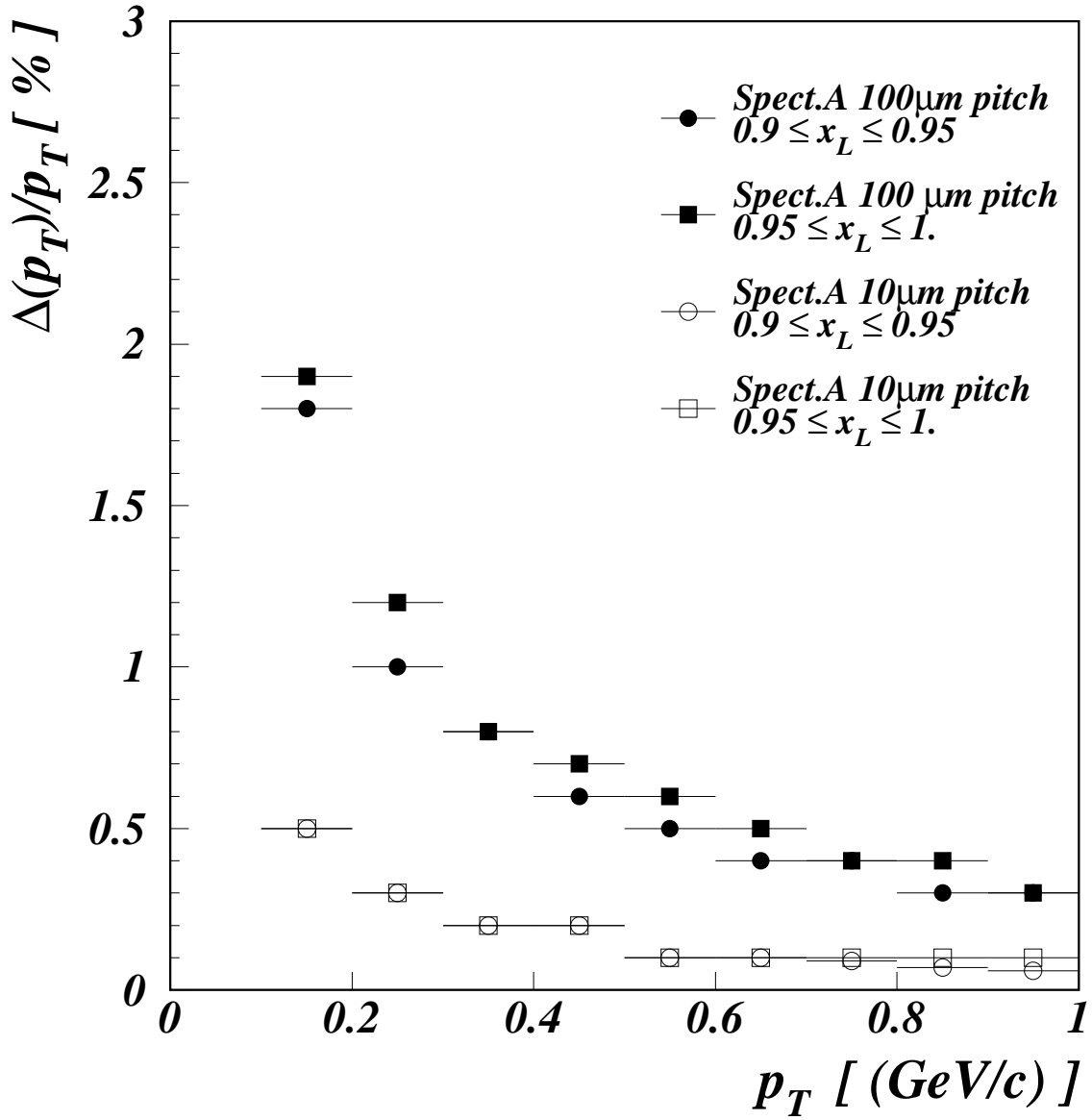


Figure 12: Transverse momentum resolution  $\frac{\Delta p_T}{p_T}$  for spectrometer A for particles generated in two different  $x_L$  bins and for 100  $\mu\text{m}$  (full symbols) or 10  $\mu\text{m}$  (open symbols) pitch detectors.

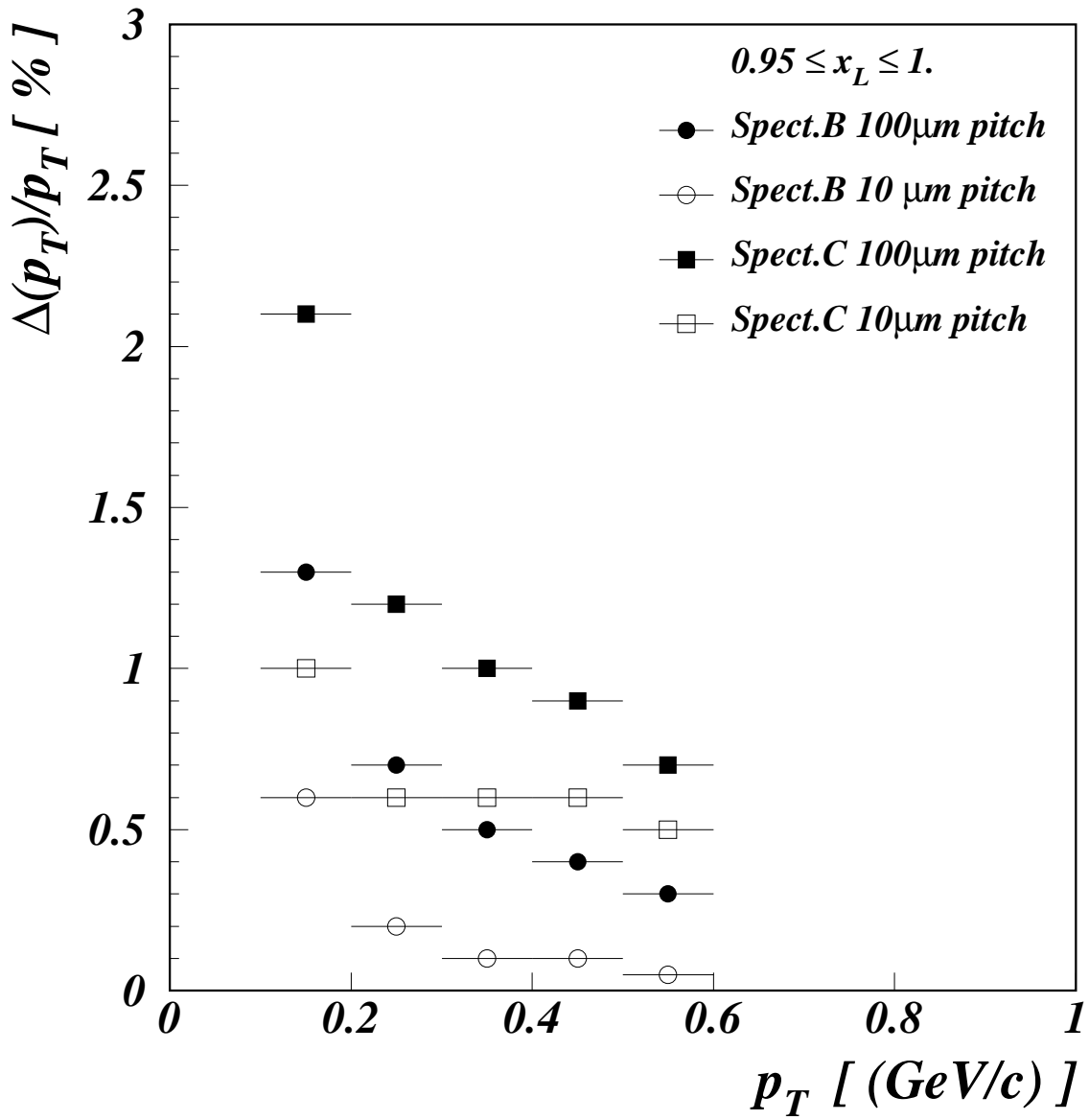


Figure 13: Transverse momentum resolution  $\frac{\Delta p_T}{p_T}$  for spectrometers *B* and *C* equipped with 100μm (full symbols) or 10μm (open symbols) pitch detectors.